

When Meta-Surfaces Meet Users: Optimization of Smart Radio Environments in 6G Sub-THz Communications

Alberto Tarable, Francesco Malandrino *Senior Member, IEEE*, Laura Dossi,
Roberto Nebuloni, Giuseppe Virone, *Senior-Member, IEEE*, Alessandro
Nordio, *Member, IEEE*

Abstract

We consider a smart radio environment where meta-surfaces are employed to improve the performance of wireless networks working at sub-THz frequencies. To this end, we propose a comprehensive mathematical channel model, taking into account both the ability of the meta-surfaces to redirect the impinging signal towards a desired direction, and the signal reflection due to large objects. We show how the design of both the meta-surface and the transmitter precoder influences the network throughput. Furthermore, we compare several algorithms to optimize the effect of the meta-surfaces in a realistic scenario. As a result, a simpler algorithm that associates network users and meta-surfaces provides a performance comparable to more complex numerical optimization methods. Simulation results suggest how many users are supported in the designed system.

Index Terms

Intelligent Reflecting Surfaces, Multiple Access, optimization, TeraHertz communication.

I. INTRODUCTION

The recent advent of the fifth generation (5G) of wireless mobile communications is revolutionizing the way we live and work, thanks to the massive increase of network capacity, to its ultra low latency, and the possibility to connect hundreds of billions of devices. To achieve this goal, millimeter wave (mm-Wave) communications combined with promising massive

A. Tarable, F. Malandrino, L. Dossi, R. Nebuloni, G. Virone, A. Nordio are with the National Research Council of Italy, Institute of Electronics, Information Engineering and Telecommunication (CNR-IEIIT), 10129 Torino, Italy (e-mail: <name>.<surname>@ieiit.cnr.it).

multiple-input multiple-output (M-MIMO) techniques have been advocated for boosting the bandwidth and the spectral efficiency, respectively.

It is also expected that the future generation of mobile communications (6G) will exploit sub-THz or THz frequency bands (usually referring to the range 0.1—10 THz [1], [2]) for indoor as well as outdoor applications involving both static and mobile users. Such bands are expected to play a major role when very high data rates are required over short distances, typically tens of meters. However, they suffer from high path loss, harsh propagation conditions, and blockages. Severe path losses can be compensated by exploiting M-MIMO techniques, which can also significantly improve the spectral efficiency at the price of an increased signal processing and hardware complexity as well as high power consumption [3].

To circumvent these problems, innovative solutions have been proposed to adapt the radio environment to the communication, thus introducing the concept of smart radio environment (SRE) [4]. SRE is a dynamically configured environment, where the interaction between radio waves and objects can be controlled in a programmable way, through the use of software-defined intelligent reflecting surfaces (IRSs) [5] made of thin layers of *meta-materials* that could be integrated within the walls of a room or of a building. An IRS is a two-dimensional *meta-surface*, composed of a large array of passive scattering elements, called *meta-atoms* [6], with specifically designed physical structure. Such meta-surfaces are able to fully control, in a software-defined manner, the phase shifts applied by individual meta-atoms to the incident signal. Macroscopically, IRSs are able to steer the impinging signal towards a desired direction and can act in synergy with M-MIMO systems. IRSs allow to move part of the intelligence of the system from the transceivers to the environment, while improving the spectrum-sharing capacity in multiuser communications, as shown in [7]. IRS applications can potentially revolutionize the classical paradigm of wireless networking, where the propagation phenomena that characterize the environment are treated as probabilistic factor that can highly affect the performance of wireless communications [6], [8] making mm-wave and THz communication technologies viable to be employed in a large class of indoor and outdoor scenarios, as envisioned by current 5G and future 6G standards [6], [8], [9].

Wireless network nodes can exploit IRSs to communicate in non-line-of-sight (NLoS) conditions, by pointing narrow radio beams towards the IRSs and let them be reflected, as exemplified in Fig. 1, thus granting connectivity even in the presence of obstacles. By smartly adjusting the phase shifts applied by the IRS elements, the reflected signals can be coherently combined at the intended receiver to improve the received power, or destructively combined at the non-intended receiver to mitigate interference, thus realizing the energy-

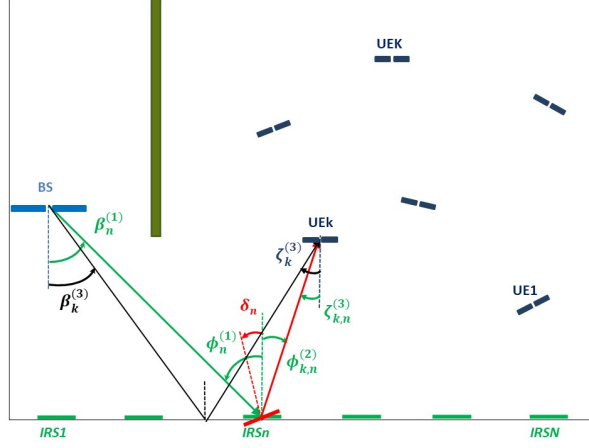


Fig. 1. An example of SRE where a BS communicates with a set of UEs by exploiting IRSs. The surfaces are electronically rotated in order to point to specific directions, hence assuring connectivity even when the LoS path between BS and UEs is unavailable. The figure shows the electronic rotation angle, δ_n , required by the n -th IRS to point its beam towards the k -th UE, as well as the path of the signal reflected by the wall (black line).

efficient so-called passive beamforming. IRSs will then become key actors in future wireless networks, by synergically interoperating with other network control strategies and signal processing techniques, such as active beamforming at the transceivers, information encoding, transmission scheduling, access control, full-duplex [10] communications, and cooperative assistance to cell-edge users [11], [12].

Most research works dealing with IRS-assisted SRE consider communications in the GHz bands and channels characterized by rich scattering, so that the radio links connecting the transmitter and the receiver to the IRSs are assumed to undergo independent fading. In such situation, the phase shifts applied by the IRS elements need to be jointly optimized in order to maximize some figure of merit (e.g., the network throughput). Such approach, however, requires each radio link to be accurately estimated and is clearly impractical and complex when the number of meta-atoms of each surface is large.

The picture changes dramatically for systems operating in the sub-THz and THz frequency bands. Indeed, although the channel at such frequencies is not yet completely characterized, some models have been proposed, such as the Saleh-Valenzuela one [13] or its extension [14, eq.(3)]. In such models, the channel matrix is given by the sum of several rank-1 terms, each of them representing a path and driven by a single random variable. However, a recent study based on indoor measurements at 142 GHz [15] highlights that all scattered components and multipath effects can be neglected. This assumption is strengthened by the fact that, when beamforming is employed, the signal power is concentrated in a specific direction,

thus further reducing the effect of multipath. In this scenario, the problem of optimizing the SRE reduces to the choice of only two design parameters for each IRS, regardless of the number of IRS elements, namely:

- the *phase gradient* among the IRS elements, which, according to the generalized Snell's law [16], determines the steering angle applied by the IRS to the impinging signal. The effect of the phase gradient is, thus, to redirect the incoming signal towards a desired direction as if the meta-surface were electronically rotated;
- a *phase shift*, which adjusts the phase of the signal reflected by each IRS in order to constructively/destructively interfere with other desired/undesired signals.

In our work, we consider the downlink of a wireless network operating in the sub-THz band, composed of a base station (BS) that communicates with a set of K user equipments (UE) through N IRSs. In our model we assume that (i) the LoS link BS–UEs is unavailable, (ii) the signal can also be reflected by large static objects (e.g., walls), and (iii) all network nodes are equipped with multiple antennas and, thus, can apply beamforming techniques. We aim at maximizing the network throughput by optimizing the IRS parameters (e.g. the phase gradient and the phase shift). Our main contributions can be summarized as follows:

- we provide a detailed communication model valid for sub-THz and THz frequency bands, accounting for the effect of the IRSs and for the signal reflection by large static objects; in particular, we characterize the asymptotic behavior of an IRS when the number of its elements is large, which is typically true even for small IRSs at sub-THz frequencies; as expected, the IRS beamforming pattern depends on its area and on the applied phase gradient and phase shift;
- we formulate an SRE optimization problem, suitable for a case in which the BS performs zero-forcing precoding, where the performance parameter is the received signal-to-noise ratio (SNR) at the UEs, and the optimization variables are phase gradients and phase shifts for all IRSs, as well as steering directions of the UE arrays;
- we propose a simple and efficient heuristic algorithm, based on the Hungarian algorithm for the linear assignment problem, which assigns a given IRS to each user; we analytically show that this approach becomes essentially optimal in the asymptotic regime where the IRSs area is large and the BS array has many antennas;
- through numerical analysis, we highlight the role of the network design parameters and their effect on the system performance; in particular, after showing that wall reflection is negligible for reasonably large IRS area, we verify the optimality of the heuristic

approach in realistic conditions and we provide design rules for the sizing of the system, in order to be able to fully exploit the angular degrees of freedom that are intrinsically available in a reference geometrical scenario.

Beyond taking into account several aspects that are most often overlooked in the literature (wall reflection, multiple antennas at the UEs), the novelty in the paper resides in the proposal of an efficient, *practical* way of performing SRE optimization, compatible with the low delay required by near-real-time scenarios, and in the analysis of its performance, whose understanding paves the way for the implementation of a veritable IRS-assisted quasi-orthogonal space-division multiple access.

The reminder of the paper is organized as follows. Section II provides an exhaustive review of the related work. In Section III, we introduce the communication model and characterize IRSs. In Section IV, we provide an asymptotic description of IRSs, which simplifies the expression of the channel matrix. Section V derives the relation between the phase gradient applied to the IRS and the resulting electronic rotation angle. Section VI proposes a set of algorithms for SRE optimization, while Section VII discusses the sensitivity of such algorithms to network parameters. Finally, Section VIII provides a set of numerical results obtained by applying the proposed algorithms to a realistic environment. Conclusions are drawn in Section IX.

A. Mathematical notation

Boldface uppercase and lowercase letters denote matrices and vectors, respectively. \mathbf{I}_k is the $k \times k$ identity matrix and $\mathbf{1}_k$ is the all-1 column vector of length k . The conjugate transpose of matrix \mathbf{A} is denoted by \mathbf{A}^H , while $[\mathbf{A}]_{i,j}$ is its (i,j) -th element. \mathbf{A}^+ and $\|\mathbf{A}\|_F$ refer, respectively, to the Moore-Penrose pseudo-inverse and the Frobenius norm of \mathbf{A} . The notation $\mathbf{A} = \text{diag}(\mathbf{a})$ specifies that the entries of the vector \mathbf{a} are the elements of the diagonal matrix \mathbf{A} . Symbols \otimes and $\mathbb{E}[\cdot]$ denote the Kronecker product and the average operator, respectively. Finally, we define the norm-1 length- M column vector $\mathbf{s}(\Delta, M, \beta)$, whose m -th entry is

$$[\mathbf{s}(\Delta, M, \beta)]_m = \frac{1}{\sqrt{M}} e^{j\pi\Delta(M-1)\sin\beta} e^{-j2\pi\Delta(m-1)\sin\beta}. \quad (1)$$

This vector represents the (normalized) spatial signature of a uniform linear array (ULA) composed of M elements spaced by Δ wavelengths as observed from the angle β , measured from the normal to the ULA.

II. RELATED WORK

Due to their promising potential in a wide range of wireless network applications, IRSs have recently attracted the interest of the research community. An overview of principles and challenges of IRSs for wireless communications is in [17], whereas [18] provides an extensive literature review ranging from the physical characterization of the IRS to the discussion of design methodologies and existing prototypes and their applications to wireless communications. Finally, [19] elaborates on aspects such as IRS passive reflection optimization, IRS channel estimation, and IRS deployment from various communication perspectives. We refer the reader to the above cited papers and to their references for a comprehensive overview of the enormous body of literature on IRSs in all their variants and applications. In the following, we give explicit references to works that deal with a scenario similar to ours.

This work focuses on sub-THz frequencies, for which highly directive beams can be generated with practically small IRSs [20]. The mathematical model of the propagation scenario adopted here for the sub-THz band is an extension to a multi-user case of the single-user IRS-enhanced environment proposed by [21], where the UE moves along a straight line. In our model, each UE is randomly displaced and it is equipped with multiple antennas to allow analog beamforming. Moreover, we adopted the design of reflective IRSs as in [22], where the far-field pathloss is derived using physical optics techniques and each IRS is interpreted as an array of subwavelength-sized diffuse scatterers that phase-align their reflected signals at the receiver and thereby achieve “anomalous” reflection.

In a multi-user scenario, optimizing the IRS is definitely more complicated than in the single-user case, and, in general, there is no optimal analytical solution. One needs then to resort to e.g. alternating optimization algorithms, iteratively optimizing over transmitted and reflected beamforming vectors, as done in [23], [24]. In many works the authors propose to jointly numerically optimize the phase shifts of each element of IRSs and the precoding matrix at the transmitter. Such methods, however, entail a high complexity, which increases with the number of IRS elements [10], [11], [21], [23], [25], and require the estimation of large channel matrices with independent entries. However, in Line of Sight (LoS) propagation on the links BS-IRSs and IRS-UEs and in far-field condition, each IRS can be characterized by two parameters, i.e., the steering angle and an eventual fixed phase shift, hence significantly reducing the complexity of optimization process, as shown in [23], [26], [27]. These properties allow for the design of efficient SRE optimization algorithms which, under some conditions, coincide with a smart one-to-one association between users and IRSs, as detailed below.

III. COMMUNICATION MODEL

We consider the downlink of a wireless network operating in the sub-THz band. The network is composed of a BS, which transmits K data streams to K users (UEs). We assume that the UEs are not in LoS with the BS and that connectivity is granted by a set of N IRS deployed along a wall, as depicted in Fig. 1. Both BS-IRS and IRS-UE links are in LoS. Additionally, the UEs receive the BS signal also through reflection from the wall. In order to simplify the discussion and the mathematical description of the system, we assume that all network nodes and IRSs have the same height above ground (2D model), in which all the relevant angles lie on the azimuth plane. The extension to a 3D scenario is straightforward and does not add significant insight on the system behavior. A detailed description of the BS, the IRSs and the UEs, as well as of the channel model, is reported below.

A. Base Station

The BS is equipped with an ULA composed of M_1 isotropic antennas, spaced by Δ_1 wavelengths. Thus, the transmitted signal, \mathbf{t} , can be represented by the $M_1 \times 1$ vector

$$\mathbf{t} = \mathbf{\Gamma} \mathbf{x}, \quad (2)$$

where $\mathbf{x} = [x_1, \dots, x_K]^T$ is the vector of transmitted symbols for the K users, supposed to have zero mean and covariance $\mathbb{E}[\mathbf{x}\mathbf{x}^H] = \mathbf{I}_K$, and $\mathbf{\Gamma}$ is a precoding matrix. We assume that the transmit power cannot exceed P_t , i.e.,

$$\mathbb{E}[\|\mathbf{t}\|_2^2] = \mathbb{E}_{\mathbf{x}} [\|\mathbf{\Gamma} \mathbf{x}\|_2^2] = \|\mathbf{\Gamma}\|_F^2 \leq P_t. \quad (3)$$

B. IRS

IRSs are composed of a large number of meta-atoms with isotropic electromagnetic properties, which behave as elementary spherical scatterers, when hit by the incident radiation from the BS. We assume that the intensity of the scattered electromagnetic field decays with the inverse of the distance, i.e., our model is intended to hold in the far-field regime [28], [22]. Moreover, we assume that the IRS are uniformly illuminated by the BS.

In our model, the n -th IRS, $n = 1, \dots, N$, is composed of L_n^2 meta-atoms [6], arranged in a $L_n \times L_n$ square grid, with total area given by

$$A_n = L_n^2 \Delta^2 \lambda^2, \quad (4)$$

where λ is the signal wavelength and Δ is the normalized meta-atom side length.

The meta-atom at position (ℓ, ℓ') in the n -th surface, $\ell, \ell' = 1, \dots, L_n$, applies a phase shift $\theta_{n,\ell,\ell'}$ to the signal impinging on it. Although, in practice, the phase shifts applied by the meta-atoms belong to a discrete set, in this work for simplicity we assume that they can take any value in $[0, 2\pi)$, as it was observed that low phase resolution entail only a small performance degradation [29] .

Many works [10], [11], [23], [21], [25] optimize the system performance by searching for the appropriate values of the phase shifts $\theta_{n,\ell,\ell'}$. However, for LoS propagation, it is straightforward to show that the optimal phase shifts of the n -th IRS are related to each other [23], [30], [26] according to the linear equation

$$\theta_{n,\ell,\ell'} = 2\pi q_n \Delta \left(\ell - 1 - \frac{L_n - 1}{2} \right) + \psi_n, \quad (5)$$

for $\ell' = 1 \dots, L_n$. By virtue of (5), the n -th IRS is able to steer the reflected signal into an arbitrary direction (depending on the parameter q_n , which is proportional to the phase gradient) as well as to apply an arbitrary phase shift (depending on ψ_n , which is the phase shift of the meta-atom at the center of the IRS). Note that (5) allows to characterize the IRS by using only two parameters, i.e., q_n and ψ_n , regardless of the number of meta-atoms L_n^2 .

C. UE

At the receiver side, we assume that the UEs are equipped with ULAs as well. Specifically, each UE ULA is composed of M_2 isotropic antennas spaced by Δ_2 wavelengths. Hence, the signal received by the k -th UE can be described by the $M_2 \times 1$ vector

$$\mathbf{r}_k = \tilde{\mathbf{H}}_k \mathbf{t} + \mathbf{z}_k, \quad (6)$$

where $\tilde{\mathbf{H}}_k$ is the $M_2 \times M_1$ channel matrix connecting the BS to the k -th UE, \mathbf{t} is the transmitted vector, given by (2), and \mathbf{z}_k is a vector of i.i.d. complex, circularly symmetric Gaussian noise samples with zero mean and variance σ^2 . We assume that the UEs can perform only analog beamforming, since they are supposed to have limited hardware complexity. Thus, the k -th UE recombines the elements of \mathbf{r}_k through the beamforming vector $\mathbf{f}_k = \mathbf{s}(\Delta_2, M_2, \alpha_k)$ and forms the output

$$y_k = \mathbf{f}_k^H \mathbf{r}_k = \mathbf{f}_k^H \tilde{\mathbf{H}}_k \mathbf{t} + \eta_k, \quad (7)$$

where $\eta_k = \mathbf{f}_k^H \mathbf{z}_k$ is a complex Gaussian random variable with zero mean and variance σ^2 , and α_k is the direction of the k -th UE beam, measured from the direction normal to the UE ULA. In conclusion, the signal received by the K UEs can be described by the vector

$$\mathbf{y} = \begin{bmatrix} y_1 \\ \vdots \\ y_K \end{bmatrix} = \underbrace{\begin{bmatrix} \mathbf{f}_1^H \tilde{\mathbf{H}}_1 \\ \vdots \\ \mathbf{f}_K^H \tilde{\mathbf{H}}_K \end{bmatrix}}_{\tilde{\mathbf{H}}} \mathbf{t} + \boldsymbol{\eta}, \quad (8)$$

where $\tilde{\mathbf{H}}$ is the overall channel matrix and $\boldsymbol{\eta} = [\eta_1, \dots, \eta_K]^T$.

D. LoS communication channel

Following the considerations made in Section I, we model the LoS channel between any two devices equipped with antenna arrays composed of, respectively, p and q elements, as the rank-1 $p \times q$ matrix

$$\mathbf{H}^{\text{LOS}} = c \mathbf{p} \mathbf{q}^H, \quad (9)$$

where the norm-1 vectors $\mathbf{p} = \mathbf{p}(\phi_r)$ and $\mathbf{q} = \mathbf{q}(\phi_t)$ represent the spatial signatures of the receive and transmit antenna arrays, respectively, in the direction specified by the angles ϕ_r and ϕ_t , measured from the direction orthogonal to the array. The coefficient c accounts for the attenuation and phase rotation due to propagation. If d is the distance between transmitter and receiver and G_1 is the array gain on one side, then the expression for c is given by

$$c = \sqrt{\frac{G_1 A}{4\pi d^2}} e^{-j\frac{2\pi}{\lambda}d} = \frac{\sqrt{G_1 G}}{4\pi d/\lambda} e^{-j\frac{2\pi}{\lambda}d}, \quad (10)$$

where the array on the other side is considered in terms of its effective area A , or in terms of its gain G . In general, the k -th UE receives the signal reflected by all IRSs as well as the one reflected by the wall, as depicted in Fig. 1. Then, the channel matrix $\tilde{\mathbf{H}}_k$ in (6) can be written as

$$\tilde{\mathbf{H}}_k = \sum_{n=1}^N \rho_n \mathbf{H}_{k,n}^{(2)} \bar{\boldsymbol{\Theta}}_n \mathbf{H}_n^{(1)} + \rho^{\text{wall}} \mathbf{H}_k^{(3)}, \quad (11)$$

where

- $\mathbf{H}_n^{(1)}$ is the $L_n^2 \times M_1$ channel matrix connecting the BS to the n -th IRS;
- $\bar{\boldsymbol{\Theta}}_n = \mathbf{I}_{L_n} \otimes \boldsymbol{\Theta}_n$ is the diagonal matrix collecting the phase shifts introduced by the meta-atoms of the n -th IRS, where $\boldsymbol{\Theta}_n = \text{diag}(e^{j\theta_{n,1,1}}, \dots, e^{j\theta_{n,L_n,1}})$, $\theta_{n,\ell,\ell'}$ being defined in (5);
- the factor ρ_n represents the reflection efficiency of the IRS;

- $\mathbf{H}_{k,n}^{(2)}$ is the $M_2 \times L_n^2$ channel matrix connecting the n -th IRS to the k -th UE;
- ρ^{wall} is the complex reflection coefficient of the wall;
- $\mathbf{H}_k^{(3)}$ is the channel matrix connecting the BS to the k -th UE, through wall reflection.

In our notation, the superscripts (1) , (2) and (3) refer to the link connecting the BS to the IRSs, the link connecting the IRSs to the UEs, and the path connecting BS and UE through wall reflection, respectively.

Now, let $d_n^{(1)}$ be the distance between the center of the BS ULA and the center of the n -th IRS. Then the matrix $\mathbf{H}_n^{(1)}$ in (11) can be written as

$$\mathbf{H}_n^{(1)} = c_n^{(1)} \bar{\mathbf{u}}_n^{(1)} \mathbf{v}_n^{(1)\text{H}}, \quad (12)$$

where

- $c_n^{(1)}$ follows (10) and is given by $c_n^{(1)} = \frac{\sqrt{M_1 A_n}}{\sqrt{4\pi d_n^{(1)}}} e^{-j\frac{2\pi}{\lambda} d_n^{(1)}}$ where A_n is given by (4);
- $\bar{\mathbf{u}}_n^{(1)} = \frac{1}{\sqrt{L_n}} \mathbf{1}_{L_n} \otimes \mathbf{s}(\Delta, L_n, \phi_n^{(1)})$ is the spatial signature of the n -th IRS, where $\phi_n^{(1)}$ is the angle of arrival (AoA) of the BS signal at the n -th IRS, measured with respect to a direction orthogonal to the surface (see Fig. 1);
- $\mathbf{v}_n^{(1)} = \mathbf{s}(\Delta_1, M_1, \beta_n^{(1)})$, where $\beta_n^{(1)}$ is the angle of departure (AoD) of the signal from the BS towards the n -th IRS, measured with respect to the direction orthogonal to the BS ULA.

Similarly, by letting $d_{k,n}^{(2)}$ be the distance between the center of the n -th IRS and the k -th UE, the matrix $\mathbf{H}_{k,n}^{(2)}$ can be specified as

$$\mathbf{H}_{k,n}^{(2)} = c_{k,n}^{(2)} \mathbf{w}_{k,n}^{(2)} \bar{\mathbf{u}}_{k,n}^{(2)\text{H}}, \quad (13)$$

where

- $c_{k,n}^{(2)} = \frac{\sqrt{M_2 A_n}}{\sqrt{4\pi d_{k,n}^{(2)}}} e^{-j\frac{2\pi}{\lambda} d_{k,n}^{(2)}}$ accounts for the free-space attenuation and the phase rotation due to propagation;
- $\mathbf{w}_{k,n}^{(2)} = \mathbf{s}(\Delta_2, M_2, \zeta_{k,n}^{(2)})$ is the spatial signature of the k -th UE ULA, where $\zeta_{k,n}^{(2)}$ is the AoA of the signal reflected by the n -th IRS, as observed from the k -th UE, measured with respect to the direction orthogonal to the UE ULA;
- $\bar{\mathbf{u}}_{k,n}^{(2)} = \frac{1}{\sqrt{L_n}} \mathbf{1}_{L_n} \otimes \mathbf{s}(\Delta, L_n, \phi_{k,n}^{(2)})$, where $\phi_{k,n}^{(2)}$ is the AoD from the n -th IRS towards the k -th UE, measured with respect to a direction orthogonal to the IRS surface.

According to the image theorem, the length of the path connecting the BS to the k -th IRS through reflection on the wall, $d_k^{(3)}$, is the sum of the BS-wall and the wall-UE path lengths. Then, the channel matrix $\mathbf{H}_k^{(3)}$ can be described as

$$\mathbf{H}_k^{(3)} = c_k^{(3)} \mathbf{w}_k^{(3)} \mathbf{v}_k^{(3)\text{H}}, \quad (14)$$

where

- $c_{k,n}^{(3)} = \frac{\sqrt{M_2 M_1 \lambda^2}}{4\pi d_k^{(3)}} e^{-j\frac{2\pi}{\lambda} d_k^{(3)}}$;
- $\mathbf{w}_k^{(3)} = \mathbf{s}(\Delta_2, M_2, \zeta_k^{(3)})$ and $\zeta_k^{(3)}$ is the AoA of the signal reflected by the wall, as observed from the k -th UE, from the direction orthogonal to the UE ULA;
- $\mathbf{v}_k^{(3)} = \mathbf{s}(\Delta_1, M_1, \beta_k^{(3)})$, and $\beta_k^{(3)}$ is the AoD of the signal that is reflected by the wall towards the k -th UE, as observed by the BS, measured from the direction orthogonal to the BS ULA.

In our work, we assume that the system has perfect knowledge of the channel matrices and of the users' positions.

IV. ASYMPTOTIC EXPRESSION OF THE CHANNEL MATRIX

The overall channel matrix $\tilde{\mathbf{H}}$ in (7) can be written in a more tractable form by letting the number of meta-atoms contained in each IRS tend to infinity, while keeping constant the surface area. This is a reasonable assumption since the number of meta-atoms in an IRS is usually large and the normalized meta-atom side length, Δ , is typically much smaller than one.

Proposition 1: As $L_1, \dots, L_N \rightarrow \infty$ while the IRS areas A_n remain constant, the matrix $\tilde{\mathbf{H}}$ tends to matrix \mathbf{H} , given by

$$\mathbf{H} = \lim_{L_1, \dots, L_N \rightarrow \infty} \tilde{\mathbf{H}} = \mathbf{M}\Psi\mathbf{V}^{(1)\text{H}} + \mathbf{T}\mathbf{V}^{(3)\text{H}}, \quad (15)$$

where $\Psi = \text{diag}(e^{j\psi_1}, \dots, e^{j\psi_N})$, $\mathbf{V}^{(1)} = [\mathbf{v}_1^{(1)}, \dots, \mathbf{v}_N^{(1)}]$, $\mathbf{V}^{(3)} = [\mathbf{v}_1^{(3)}, \dots, \mathbf{v}_K^{(3)}]$, \mathbf{M} is a $K \times N$ matrix whose elements are given by

$$[\mathbf{M}]_{k,n} = \frac{b_{k,n} \rho_n \sqrt{M_1 M_2} A_n}{4\pi d_n^{(1)} d_{k,n}^{(2)} e^{j\frac{2\pi}{\lambda} (d_n^{(1)} + d_{k,n}^{(2)})}} \text{sinc}\left(\frac{\sqrt{A_n}}{\lambda} s_{k,n}\right). \quad (16)$$

\mathbf{T} is a diagonal matrix whose k -th diagonal element is given by

$$[\mathbf{T}]_{k,k} = b_k \rho^{\text{wall}} c_k^{(3)}, \quad (17)$$

having defined

$$b_{k,n} \triangleq \frac{\text{sinc}(\Delta_2 M_2 (\sin \alpha_k - \sin \zeta_{k,n}))}{\text{sinc}(\Delta_2 (\sin \alpha_k - \sin \zeta_{k,n}))},$$

$$b_k \triangleq \frac{\text{sinc}(\Delta_2 M_2 (\sin \alpha_k - \sin \zeta_k))}{\text{sinc}(\Delta_2 (\sin \alpha_k - \sin \zeta_k))},$$

and

$$s_{k,n} = \sin \phi_n^{(1)} - \sin \phi_{k,n}^{(2)} - q_n. \quad (18)$$

Proof: See Appendix A. ■

We make the following remarks about (16):

- $s_{k,n}$ is related to the misalignment of the k -th UE w.r.t. the beam reflected by the n -th IRS, whose direction of maximum radiation corresponds to $s_{k,n} = 0$;
- as it can be expected, (16) is similar to the bistatic radar equation when a tilted flat plate is considered as target;
- each IRS generates a beam whose width is proportional to the ratio $\lambda/\sqrt{A_n}$. Therefore, larger surfaces generate narrower beams.

In the following, we will replace the matrix $\tilde{\mathbf{H}}$ with its asymptotic expression \mathbf{H} given in (15), so that the received signal takes the form

$$\mathbf{y} = \mathbf{H}\mathbf{t} + \boldsymbol{\eta}. \quad (19)$$

V. ELECTRONIC ROTATION OF THE IRSS

The macroscopic effect of the phase gradient applied to the IRS meta-atoms is to *electronically rotate* the IRS with respect to its physical orientation, according to the generalized Snell's law [16]. By electronic rotation, the beam generated by the IRS can be steered to point to an arbitrary direction.

The angle of electronic rotation of the n -th IRS, δ_n , only depends on the gradient of the phase shift in (5), i.e. on the parameter q_n . In order to map the parameter q_n into the corresponding rotation angle of the IRS, we make the key observation that the term $s_{k,n}$ in (18) can be rewritten as

$$s_{k,n} = \sin(\phi_n^{(1)} - 2\delta_n) - \sin(\phi_{k,n}^{(2)}), \quad (20)$$

where we recall that the angles $\phi_n^{(1)}$ and $\phi_{k,n}^{(2)}$ represent the AoA of the signal received at the n -th IRS and the AoD from the n -th IRS towards the k -th UE, respectively, measured in the azimuth plane and with respect to a direction orthogonal to the surface. Given the geometry of the network (i.e., the position of the BS, of the IRSs and of the UEs), such quantities are known.

Note that the angles $\phi_n^{(1)} - \delta_n$ and $\phi_{k,n}^{(2)} + \delta_n$ are the AoA and the AoD, respectively, *as seen from the electronically rotated surface* (see Figure 1 for details). The relation between the phase gradient, q_n , and the rotation angle, δ_n , can be immediately derived by equating (18) and (20). In the following, we will drop the expression for $s_{k,n}$ in (18) in favor of (20), since the angle δ_n has a clearer geometric interpretation than q_n . Thus, if we want to point the beam generated by the n -th surface towards the k -th UE, we must set the rotation angle δ_n in (20), so as to have $s_{k,n} = 0$.

VI. COMMUNICATION SYSTEM OPTIMIZATION

In this section, we face the design of the communication system by a pragmatic approach divided into two steps:

- 1) we first design the signal transmitted by the BS, by selecting a suitable precoder, $\mathbf{\Gamma}$;
- 2) given $\mathbf{\Gamma}$, we define an optimization problem in which the performance parameter is the SNR received by the UEs, and the optimization variables are $\boldsymbol{\delta} = [\delta_1, \dots, \delta_N]^T$, $\boldsymbol{\psi} = [\psi_1, \dots, \psi_N]^T$, and $\boldsymbol{\alpha} = [\alpha_1, \dots, \alpha_K]^T$, characterizing the rotations and phase shifts of the IRSs, and the direction of the beams generated by the UE ULAs, respectively. To solve this problem, we first provide a numerical approach based on the Newton-Raphson method, outlined in Sec. VI-B, and then, we propose a heuristic optimization algorithm, described in Sec. VI-C.

A. Signal precoding at the BS

Substituting (2) into (19) we can rewrite the received signal as

$$\mathbf{y} = \mathbf{H}\mathbf{\Gamma}\mathbf{x} + \boldsymbol{\eta}. \quad (21)$$

The precoding matrix $\mathbf{\Gamma}$ should be designed so as to adapt the transmitted signal to the propagation environment. Several choices are possible: for example it can be designed to maximize the SINR at the receivers or to null out the interference among UEs, at a price of a reduction of SINR. In this work we consider zero-forcing (ZF) precoding, similarly to what done in [31]. Specifically, we will assume in the following that $\min(M_1, N) \geq K$. Under this hypothesis, we can choose $\mathbf{\Gamma}$ to satisfy

$$\mathbf{H}\mathbf{\Gamma} = a\mathbf{Q}^{1/2}, \quad (22)$$

where \mathbf{Q} is a diagonal matrix and a is a coefficient. Indeed, by substituting (22) in (21) we observe that the effect of the precoder is to diagonalize the end-to-end channel matrix and, by consequence, make the UEs' channels orthogonal. By solving (22) for $\mathbf{\Gamma}$, the precoder can be written as

$$\mathbf{\Gamma} = a\mathbf{H}^+\mathbf{Q}^{1/2}, \quad (23)$$

where $\mathbf{H}^+ = \mathbf{H}^H (\mathbf{H}\mathbf{H}^H)^{-1}$ is the pseudo-inverse of \mathbf{H} and $a = \frac{\sqrt{P_t}}{\|\mathbf{H}^+\mathbf{Q}^{1/2}\|_F}$ in order to meet the transmit power constraint in (3). With this precoder choice, the received SNR at the k -th UE is given by

$$\text{SNR}_k = \frac{P_t q_k}{\sigma^2 \|\mathbf{H}^+\mathbf{Q}^{1/2}\|_F^2}, \quad (24)$$

where q_k is the k -th diagonal element of \mathbf{Q} . The SNR in (24) corresponds to a spectral efficiency per user of

$$R_k = \log_2(1 + \text{SNR}_k) , \quad (25)$$

expressed in bit/s/Hz. Note that, by varying q_k it is possible to provide the UEs with different quality of service, i.e., different values of R_k . In the special case $\mathbf{Q} = \mathbf{I}$, all users achieve the same spectral efficiency. While the expression for $\mathbf{\Gamma}$ in (23) is suboptimal in terms of achievable rate, it has the advantage of completely removing interference among streams at the UEs and, more importantly, allows for a relatively simple optimization of the SNR received by the UEs, as shown in the next subsection.

B. SRE optimization

In our design, the goal of SRE optimization is the maximization of received SNR at the UEs. Let $\boldsymbol{\xi} = [\boldsymbol{\delta}^\top, \boldsymbol{\psi}^\top, \boldsymbol{\alpha}^\top]^\top \in [0, 2\pi]^{2N+K}$. For a given matrix \mathbf{Q} , in view of (24), we face the following optimization problem

$$\text{SNR}_k^{\text{opt}} = \max_{\boldsymbol{\xi}} \text{SNR}_k = \frac{P_t q_k}{\sigma^2 \min_{\boldsymbol{\xi}} \|\mathbf{H}^+ \mathbf{Q}^{1/2}\|_F^2} . \quad (26)$$

It turns out that SNR maximization is equivalent to minimizing the term $\|\mathbf{H}^+ \mathbf{Q}^{1/2}\|_F$ which, in general, is not a convex function of $\boldsymbol{\xi}$. The optimal value for $\boldsymbol{\xi}$, in the following denoted by $\boldsymbol{\xi}_{\text{opt}}$ will then be given by

$$\boldsymbol{\xi}_{\text{opt}} = \arg \min_{\boldsymbol{\xi} \in [0, 2\pi]^{2N+K}} \|\mathbf{H}^+ \mathbf{Q}^{1/2}\|_F^2 = \arg \min_{\boldsymbol{\xi} \in [0, 2\pi]^{2N+K}} \text{Tr} \{ (\mathbf{H}\mathbf{H}^\text{H})^{-1} \mathbf{Q} \} . \quad (27)$$

Note that \mathbf{H} is defined by (15), (16), (17), and (20). In particular \mathbf{H} depends on $\boldsymbol{\delta}$ only through matrix \mathbf{M} , on $\boldsymbol{\alpha}$ through matrices \mathbf{M} and \mathbf{T} , while it depends on $\boldsymbol{\psi}$ only through matrix $\boldsymbol{\Psi}$. Finally, matrices $\mathbf{V}^{(1)}$ and $\mathbf{V}^{(3)}$ are constant, given the geometry of the system. Let $f(\boldsymbol{\xi}) = \text{Tr} \{ (\mathbf{H}\mathbf{H}^\text{H})^{-1} \mathbf{Q} \}$. We can solve numerically (27) by the iterative Newton-Raphson method. Given a starting point $\boldsymbol{\xi}^{(0)}$, the h -th estimate of $\boldsymbol{\xi}_{\text{opt}}$, $h = 1, 2, \dots$ is given by

$$\boldsymbol{\xi}^{(h)} = \boldsymbol{\xi}^{(h-1)} - \left[\boldsymbol{\mathcal{H}} \left(\boldsymbol{\xi}^{(h-1)} \right) \right]^{-1} \nabla f \left(\boldsymbol{\xi}^{(h-1)} \right) , \quad (28)$$

where $\boldsymbol{\mathcal{H}} = \frac{\partial^2 f}{\partial \boldsymbol{\xi} \partial \boldsymbol{\xi}^\top}$ is the Hessian matrix of $f(\boldsymbol{\xi})$. The expressions for ∇f and $\boldsymbol{\mathcal{H}}$ can be obtained in closed form. A detailed derivation is reported in Appendix B.

Iterations of the Newton-Raphson algorithm stop when the magnitude of the increment from one iteration to the next one falls below a predetermined threshold. Since $f(\boldsymbol{\xi})$ is not convex, several different starting points need to be taken, and the final approximation of $\boldsymbol{\xi}_{\text{opt}}$ is the (local) minimum point that yields the smallest value of $f(\boldsymbol{\xi})$.

C. Heuristic SRE optimization

Owing to the complexity of the optimization problem defined in (26), we propose a simpler, heuristic approach to environment optimization. Specifically, we make the key observation that, in most practical cases, a given IRS serves a single user, properly chosen. By restricting our attention to a solution where each UE is associated with one IRS, we are able to solve a substantially simpler problem, at a modest cost in terms of distance from the optimum, as shown in Section VIII. Formally, this can be done by defining the map

$$\mathcal{M} : \{1, \dots, K\} \rightarrow \{1, \dots, N\}, \quad (29)$$

which associates UE k to IRS $\mathcal{M}(k)$. In practice, this means that the $\mathcal{M}(k)$ -th IRS should be rotated so as to point its beam in the direction of the UE k and that the UE k steers its ULA so that it points towards the $\mathcal{M}(k)$ -th IRS. This criterion is particularly suited when the surfaces are sufficiently large and the UE ULAs have enough antennas so that the beam reflected by IRS $\mathcal{M}(k)$ reaches UE k without interfering with other UEs.

In the heuristic environment optimization, given the map \mathcal{M} , we set

$$\delta_{\mathcal{M}(k)} = \frac{\phi_{\mathcal{M}(k)}^{(1)} - \phi_{k, \mathcal{M}(k)}^{(2)}}{2}, \quad (30)$$

which yields $s_{k, \mathcal{M}(k)} = 0$ in (20), and on the UE side

$$\alpha_k = \zeta_{k, \mathcal{M}(k)}, \quad (31)$$

so that $b_{k, \mathcal{M}(k)} = 1$ in (16). Regarding phase shifts, we set $\psi_{\mathcal{M}(k)}$ so that the reflected waves from the IRS and from the wall arrive to the UE with the same phase, to obtain constructive interference.

It is worth noting that, if $N > K$, there are $N - K$ IRSs which are not associated to any user. While in a scenario with small surfaces and single-antenna UEs, the contribution of these IRSs can be relevant, with narrow reflected beams and directive UE arrays, their effect can be neglected, as we will see in Section VIII. If the n -th IRS is not associated to any UE, we conventionally set $\delta_n = 0$ and $\psi_n = 0$.

Let $\xi = \xi(\mathcal{M})$ be the value of ξ resulting from a given map \mathcal{M} . The proposed heuristic algorithm then consists in finding the optimal map, \mathcal{M}_{opt} , satisfying

$$\mathcal{M}_{\text{opt}} = \arg \min_{\mathcal{M}} \|\mathbf{H}_{\text{heu}}^+ \mathbf{Q}^{1/2}\|_{\text{F}}, \quad (32)$$

where \mathbf{H}_{heu} is the channel matrix obtained by setting $\xi = \xi(\mathcal{M})$. Notice that, since there are $N!/(N - K)!$ possible maps, an exhaustive search of \mathcal{M}_{opt} is possible only for small-size scenarios.

VII. SENSITIVITY OF SRE OPTIMIZATION TO SYSTEM PARAMETERS

In this section, we analyze the sensitivity of SRE optimization, as described in the previous section, to some system parameters. In particular, we consider the impact on the received SNR in (24) of the size of the ULA arrays at the BS and at the UEs, and of the IRS areas. Moreover, in a properly defined limiting regime, we derive a simplified criterion for optimization.

A. Impact of the number of ULA array elements

We first notice that the number of elements of the BS ULA, M_1 , appears in matrix $\mathbf{V}^{(1)}$ whose n -th column is given by $\mathbf{v}_n^{(1)} = \mathbf{s}(\Delta_1, M_1, \beta_n^{(1)})$. Such matrix only depends on the geometry of the system and is not affected by electronic IRS rotation or phase shifts.

From (24), the received SNR depends on $\mathbf{V}^{(1)}$ through $\mathbf{V}^{(1)\text{H}}\mathbf{V}^{(1)}$, whose (n, n') entry is given by

$$\mathbf{v}_n^{(1)\text{H}}\mathbf{v}_{n'}^{(1)} = \frac{1}{M_1} \frac{\sin\left(2\pi\Delta_1 M_1(\sin\beta_n^{(1)} - \sin\beta_{n'}^{(1)})\right)}{\sin\left(2\pi\Delta_1(\sin\beta_n^{(1)} - \sin\beta_{n'}^{(1)})\right)}. \quad (33)$$

Now, for a given geometry, the AoDs $\beta_1^{(1)}, \dots, \beta_N^{(1)}$ are fixed and we suppose that $\beta_n^{(1)} \neq \beta_{n'}^{(1)}$ for $n \neq n'$. Thus:

$$\left| \mathbf{v}_n^{(1)\text{H}}\mathbf{v}_{n'}^{(1)} \right| \leq \frac{1}{M_1 \left| \sin\left(2\pi\Delta_1(\sin\beta_n^{(1)} - \sin\beta_{n'}^{(1)})\right) \right|} \xrightarrow{M_1 \rightarrow \infty} 0 \quad (34)$$

for $n \neq n'$. This implies that $\lim_{M_1 \rightarrow \infty} \mathbf{V}^{(1)\text{H}}\mathbf{V}^{(1)} = \mathbf{I}_N$. Similarly, the parameter M_1 also appears in $\mathbf{V}^{(3)}$. Then, provided that $\beta_k^{(3)} \neq \beta_{k'}^{(3)}$ for $k \neq k'$, $\lim_{M_1 \rightarrow \infty} \mathbf{V}^{(3)\text{H}}\mathbf{V}^{(3)} = \mathbf{I}_K$. Finally, if $\beta_n^{(1)} \neq \beta_k^{(3)}$ for every pair of k and n , $\lim_{M_1 \rightarrow \infty} \mathbf{V}^{(1)\text{H}}\mathbf{V}^{(3)} = \mathbf{0}_{N \times K}$. As a consequence, when IRSs and UEs are angularly separated with respect to the BS,

$$\|\mathbf{H}^+\mathbf{Q}^{1/2}\|_{\text{F}}^2 = \text{Tr}\{(\mathbf{H}\mathbf{H}^{\text{H}})^{-1}\mathbf{Q}\} \xrightarrow{M_1 \rightarrow \infty} \text{Tr}\{(\mathbf{M}\mathbf{M}^{\text{H}} + \mathbf{T}\mathbf{T}^{\text{H}})^{-1}\mathbf{Q}\}. \quad (35)$$

Notice that, in this asymptotic regime, the received SNR becomes independent of the phase shifts ψ . This happens because, when M_1 gets large, the columns of $\mathbf{V}^{(1)}$ become orthogonal and it is the precoder that allows to properly set the phases of the signals impinging to each IRS. Summarizing, we expect that *for increasing transmit array size, the impact on received SNR of phase shifts decreases until it becomes negligible*.

¹The larger M_1 , the narrower the BS transmitted beam. Thus, for a too large value of M_1 , the hypothesis that the transmitted beam uniformly illuminates the IRSs does not hold. However, as we will see in Section VIII, for a realistic scenario, this case does not happen.

B. Impact of IRS areas, A_n

As already observed, from the expression of $[\mathbf{M}]_{k,n}$ in (16) it can be seen that the width of the beam reflected by the n -th IRS depends on its area, A_n . In particular, for $\frac{\sqrt{A_n}}{\lambda} \rightarrow \infty$:

$$[\mathbf{M}]_{k,n} \rightarrow \frac{a_n^{(1)} a_{k,n}^{(2)} b_{k,n} \rho_n \sqrt{M_1 M_2} A}{4\pi d_n^{(1)} d_{k,n}^{(2)} e^{j\frac{2\pi}{\lambda}(d_n^{(1)} + d_{k,n}^{(2)})}} \delta[s_{k,n}] , \quad (36)$$

where $\delta[x] = 1$ for $x = 0$ and $\delta[x] = 0$ otherwise. Thus, it turns out that the n -th IRS contributes to the signal received by the k -th UE only if it points towards it. As a consequence, we expect that *for IRSs with large area (compared to λ^2), each IRS should be rotated to point in the direction of a given UE.*

C. SRE optimization algorithms in the asymptotic regime

In the doubly asymptotic regime $M_1, A_n \rightarrow \infty$, SRE optimization becomes easier to state and to solve. Indeed, thanks to (35), the optimization problem in (27) reduces to

$$\tilde{\boldsymbol{\xi}}_{\text{opt}} = \arg \min_{\tilde{\boldsymbol{\xi}} \in [0, 2\pi]^{N+K}} \text{Tr} \{ (\mathbf{M}\mathbf{M}^H + \mathbf{T}\mathbf{T}^H)^{-1} \mathbf{Q} \} , \quad (37)$$

where $\tilde{\boldsymbol{\xi}} = [\boldsymbol{\delta}, \boldsymbol{\alpha}]^T$. Moreover, if we suppose that the users are angularly separated, then, by (36), we obtain that $[\mathbf{M}]_{k,n} \neq 0$ if and only if $n = \mathcal{M}(k)$. As a consequence, $\mathbf{M}\mathbf{M}^H$ becomes diagonal and the heuristic problem becomes

$$\mathcal{M}_{\text{opt}}^\infty = \arg \min_{\mathcal{M}} \omega(\mathcal{M}) , \quad (38)$$

where

$$\omega(\mathcal{M}) = \sum_{k=1}^K \left(|[\mathbf{M}]_{k, \mathcal{M}(k)}|^2 + |[\mathbf{T}]_{k,k}|^2 \right)^{-1} q_k . \quad (39)$$

The above is an assignment problem whose weights are the sums of the squared magnitudes of the entries of \mathbf{M} and \mathbf{T} . To obtain the optimal solution of the above problem, we can resort to, e.g., the Hungarian algorithm [32]. It is important to highlight how the Hungarian algorithm has very low, namely, cubic complexity [32], hence, it can be efficiently used for realistically-sized problem instances.

In the next section, we will show when, in a realistic scenario, conditions for the asymptotic regime are met. In such conditions, the heuristic algorithm in its simplified version (38)-(39) represents a feasible way of SRE optimization. It is worth noting that the zero-forcing precoder $\boldsymbol{\Gamma}$ tends to be a simple equalizing beamformer in the asymptotic regime, since the channels corresponding to the K users become orthogonal by themselves, and $\boldsymbol{\Gamma}$ tends to split the power among the different channels in order to meet the relative quality of service dictated by matrix \mathbf{Q} .

VIII. NUMERICAL RESULTS

In this section, we provide some insight on the system behavior through numerical results. In particular, we discuss the performance of the optimization algorithms proposed in Section VI and we show the influence of the system parameters on the SNR at the UEs. We consider the test scenario in Fig. 3, depicting an area of 100 m^2 , whose vertices, in the (x, y) plane, are the points $(-5, 0)$, $(5, 0)$, $(-5, 10)$ and $(5, 10)$ (all coordinates expressed in meters). The BS is located at coordinates $(-5, 5)$. The transmitted signal has bandwidth $B = 100 \text{ MHz}$ and carrier frequency $f_0 = 0.1 \text{ THz}$, corresponding to the wavelength $\lambda = 3 \text{ mm}$. The transmit power is $P_t = 1 \text{ W}$ and we set $\mathbf{Q} = \mathbf{I}$, i.e., the transmit power is partitioned among the K data streams so that, by applying the ZF precoding filter $\mathbf{\Gamma}$ in (23), all users have the same SNR. Finally, the antenna separation of the BS ULA is $\Delta_1 = \lambda/2$.

The N IRSs, denoted by the labels IRS1, \dots , IRS N , have square shape, area $A_n = A$ and are deployed along a wall located at $x = 0$, symmetrically w.r.t. the y -axis. The IRSs centers are equally spaced by D meters, depending on N . Specifically, in our setup, we consider $D = [7.5, 2.5, 1.25, 0.8, 0.625, 0.48, 0.4, 0.36, 0.3] \text{ m}$ for $N = [2, 4, 8, 12, 16, 20, 24, 28, 32]$, respectively. We assume ideal reflection at the IRSs, i.e., the ratio between the amplitude of incident and reflected waves for the IRSs, ρ_n , is set to 1.

The K UEs, denoted by the labels UE1, \dots , UE K , are distributed according to a uniform random distribution in the area whose vertices are the points $(0, 0)$, $(5, 0)$, $(5, 10)$ and $(0, 10)$. The elements of the UE ULAs are also separated by $\Delta_2 = \lambda/2$ and the noise variance at the receivers is set to $\sigma^2 = N_0 B$ where $N_0 = -174 \text{ dBm/Hz}$.

The BS-IRSs and IRSs-UEs links are supposed to be LoS whereas no direct LoS component is supposed to exist between the BS and the UEs. We consider, however, the effect of the wall, which reflects the BS signal, as shown in Fig. 1. The reflected signal is subject to the complex reflection coefficient ρ^{wall} which, in general, depends on the AoA of the BS signal on the wall. In our simulations, we have used the model described in Figure 2, which holds for plasterboard surfaces at 100GHz and vertical polarization [33].

In the simulation setup, we consider the following techniques to solve the problem in (26)

- the joint optimization of the IRS electronic rotation angles, δ , of the phase shifts, ψ , and of the UE beam directions, α , by employing the Newton-Raphson algorithm, in the following referred to as “NRP”;
- the joint optimization of the IRS electronic rotation angles and of the UE beam directions by employing the Newton-Raphson algorithm, while setting to zero the IRS phase shifts.

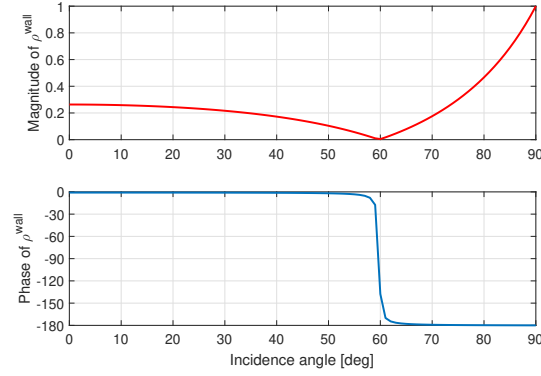


Fig. 2. Amplitude (above) and phase (below) of the complex reflection coefficient ρ^{wall} , for plasterboard panels, plotted versus the AoA of the BS signal. The incidence angle is measured from the direction orthogonal to the wall.

This technique, denoted as “NR”, solves (26) by imposing $\psi = 0$;

- the heuristic optimization algorithm (HOP) described in Section VI-C and based on the evaluation of (38)-(39). This algorithm takes the phase shifts, ψ , into account for the optimization.

Since, in general, the expression of the SNR in (24) is not convex in ξ , for each realization of the UE positions, we perform $U = 1000$ runs of the NR and NRP algorithms, each characterized by a different, randomly generated, starting point $\xi_u^{(0)}$, $u = 1, \dots, U$ and an output SNR_u . Then, for each realization of the UE positions, the SNR provided by the algorithms is $\max_u \text{SNR}_u$.

The numerical results are organized as follows: in Section VIII-A, we show examples of the radiation patterns emitted by the IRSs and by the BS ULA, while in Section VIII-B we compare the performance of the above optimization techniques in terms of the achieved SNR. Finally, in Section VIII-C, we evaluate the impact of the system parameters on the network throughput.

A. Radiation patterns

We start by analyzing the scenario depicted in Fig. 3. We consider a BS, whose ULA has $M_1 = 32$ antenna elements, $N = 4$ IRSs of area $A = 100 \text{ cm}^2$ deployed along a wall (represented by the x axis) and $K = 4$ UEs, whose positions are fixed, and are equipped with isotropic antennas ($M_2 = 1$). The contribution of the signal reflected by the wall is neglected and the dashed lines indicate the BS-IRS LoS links. The HOP algorithm applied to this scenario selects the IRS-UE assignment depicted in the figure by solid lines. Specifically, the IRSs 1,2,3, and 4 are electronically rotated so as to point their beams, respectively, towards

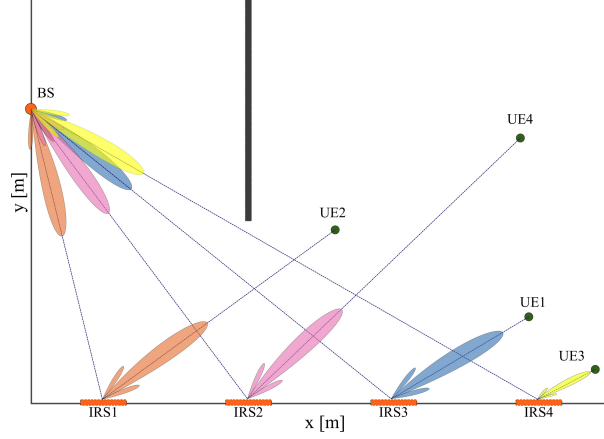


Fig. 3. An example of the system geometry considered in Section VIII for the specific case $K = 4$, $M_2 = 1$ and $N = 4$. When the BS ULA has $M_1 = 32$ elements and the IRS have area $A=100 \text{ cm}^2$, the optimal IRS-UE assignments selected by the HOP algorithm are represented by different colours solid segments. The signal reflected by the wall is not shown.

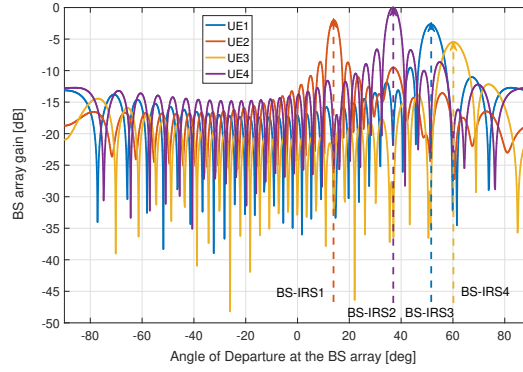


Fig. 4. BS array gain, $|\gamma_k|^2$, for each of the K data streams transmitted in the scenario depicted in Fig. 3. The dashed arrows indicate the directions of the IRSs as observed from the BS.

UEs 2,4,1, and 3. Referring to (38), this assignment corresponds to the map $\mathcal{M}_{\text{opt}}^\infty(1) = 3$, $\mathcal{M}_{\text{opt}}^\infty(2) = 1$, $\mathcal{M}_{\text{opt}}^\infty(3) = 4$, and $\mathcal{M}_{\text{opt}}^\infty(4) = 2$.

Note that since $M_2 = 1$, the UE antennas are isotropic and, thus, the parameter α (giving the direction of the UE beams) does not come into play. To get insight on how the energy of the K signals transmitted by the BS is distributed among the IRSs, in Figure 4 we show the gains $\mathbf{s}(\Delta_1, M_1, \beta)^H \gamma_k$, $k = 1, \dots, K$, plotted versus the AoD β from the BS ULA. We recall that the vectors γ_k are the columns of the precoder $\mathbf{\Gamma}$, which is matched to the channel matrix obtained with the parameters yielded by the HOP algorithm.

As can be observed from Fig. 4, the radiation pattern for the data stream intended for UE1 clearly shows a main lobe in the direction of the IRS3 since such surface steers the signal towards UE1. Similarly, the radiation patterns for UE2, UE3 and UE4 show peak values in the direction of IRS1, IRS4 and IRS2, respectively. These patterns are clearly in accordance

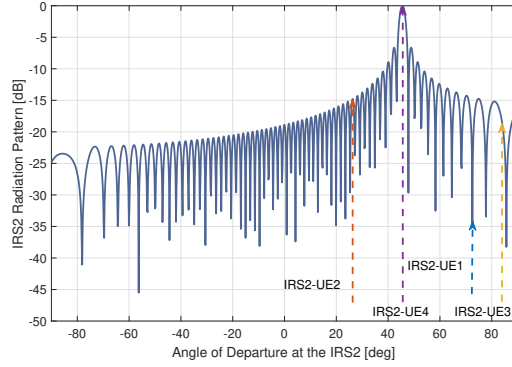


Fig. 5. Radiation pattern of IRS2, whose size is $A = 100 \text{ cm}^2$, for the IRS-UE assignment as shown in Fig. 3. The dashed lines indicate the directions of the users as observed the IRS.

to the IRS-UE assignment selected by HOP and depicted in Fig. 3.

Note that, in general, the signal illuminating an IRS can carry the contribution of more data streams. This is, for example, the case of IRS2, which receives the signal intended for UE4 and also a contribution of the signal intended for UE2, albeit 10dB lower. This interference is, however, canceled out at the UEs by means of destructive interference, thanks to a proper setting of the IRS phase shifts. Thus, the overall user channels are orthogonal, as granted by the ZF filter.

As mentioned in Section IV, the area of an IRS affects the beamwidth of its emitted radiation pattern. For an IRS area of 100 cm^2 , as in the scenario depicted in Fig. 3, the first-null beamwidth is about 2° (16). This observation is supported by Fig.5, which shows the radiation pattern emitted by IRS2, plotted versus the direction normal to the IRS in the azimuth plane. The dashed lines indicate the directions of the users as observed by IRS2. As can be seen, most of the energy is reflected towards UE4, a small fraction of it (about -15dB) also reaches the other UEs, but is canceled out by means of destructive interference, as explained before. The figure shows also that the IRS is able to steer the signal according to the *generalized* Snell's law. Indeed, the AoA of the BS signal is 36.8 degrees, while the AoD towards the UE is 45.5 degrees. If the IRS was replaced by a dumb mirror, such angles would coincide, according to Snell's law.

B. Performance comparison of the optimization algorithms

We now investigate the performance of the optimization algorithms described in Section VIII and the impact of the system parameters on the received SNR. First of all, we measure the effect of the signal reflected by the wall. We therefore consider a simple scenario

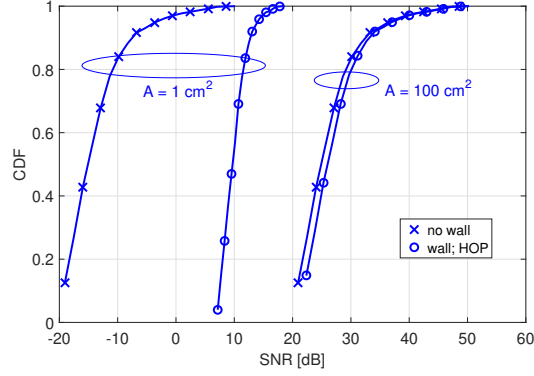


Fig. 6. Cdf of the SNR at the UEs for $M_1 = 4$ BS antenna elements, $M_2 = 1$ UE antenna elements, $N = 1$ IRSs, $K = 1$ UEs, IRS area $A = 1 \text{ cm}^2$ (solid lines) and $A = 100 \text{ cm}^2$ (dashed lines) with or without wall reflection.

where a single UE ($K = 1$) equipped with an isotropic antenna ($M_2 = 1$) is served by a single IRS ($N = 1$). The BS ULA has $M_1 = 4$ elements. In this case, the optimization of the environment consists only in the proper choice of the electronic rotation δ_1 of the IRS and of the phase shift ψ_1 , since for $M_2 = 1$ there is no beam direction to be optimized at the UE. The optimal electronic rotation of the IRS is achieved when the beam reflected by the IRS points towards the UE. So, given the UE position, we choose δ_1 so as to null $s_{1,1}$ in (20). Moreover, in the absence of a signal reflected by the wall, the value of the IRS phase shift ψ_1 does not affect the received SNR, whereas, in its presence, it should be set so as to ensure constructive interference at the UE. The cumulative density function (cdf) of the SNR at the UE for IRSs of areas $A = 1 \text{ cm}^2$ and $A = 100 \text{ cm}^2$ is reported in Fig. 6. For $A = 1 \text{ cm}^2$, the figure shows that the SNR is dominated by the contribution of the signal reflected by the wall, which yields a gain of about 25 dB with respect to the scenario without wall reflection. Instead, for $A = 100 \text{ cm}^2$, the beneficial contribution of the wall is limited to about 1.5 dB. This means that IRSs with area $A = 100 \text{ cm}^2$ can help in situations where there are no natural signal reflectors in the environment. Instead, small IRSs provide little contribution to the received power. Note also that, in the absence of wall reflection, by increasing the IRS area from 1 cm^2 to 100 cm^2 we obtain 40 dB improvement in the SNR. This is expected since, from (16), the SNR depends on A^2 .

In Fig. 7 we consider the same scenario as in Fig. 6 where, however, the UE is endowed with an ULA with $M_2 = 4$ elements. In this case, the received SNR also depends on the direction α_1 of the beam of the UE ULA and, therefore, the SNR optimization in (26) is not anymore trivial. We show the performance of the different optimization algorithms in terms of achieved SNR. While all algorithms agree that the IRS should point its beam towards the

UE, they perform divergent choices for the angle α_1 . Specifically,

- the NRP algorithm rotates the UE beam so as to maximize the received energy at the UE. The optimal direction is, in general, in between the directions of the beams reflected by the IRS and by the wall. Also, NRP adjusts the IRS phase shift, so as to create constructive interference of the two signals at the UE;
- the NR algorithm operates similarly to NRP, but it does not optimize the IRS phase shift;
- the HOP algorithm points the UE beam towards the IRS, neglecting the effect of the wall.

We observe that the performance of the three algorithms is equivalent in absence of the signal reflected by the wall. However, significant differences arise when the IRS area is small and in presence of the wall. For $A = 1 \text{ cm}^2$, the HOP algorithm performs poorly since it points the UE beam towards the IRS, which provides a very weak signal compared to that reflected by the wall. Instead, NRP and NR perform similarly and in general steer the UE beam towards the stronger energy source. Instead, for $A = 100 \text{ cm}^2$, the HOP algorithm performs identically to the much more complex NRP and NR algorithms. This means that a simple decision-making approach on the IRS-UE association can provide optimal results. HOP represents, therefore, an attractive solution for its simplicity and effectiveness.

We also observe that, for $A = 100 \text{ cm}^2$, the curves in Fig. 7 show a 6 dB gain w.r.t. those shown in Fig. 6. Such gain is achieved by the UE ULA ($M_2 = 4$) with respect to an isotropic antenna. Finally, from the above results, we conclude that IRSs with an area as large as 100 cm^2 are required, in order to collect and reflect enough signal energy to dominate the effect of the wall. In the following, we concentrate on the case $A = 100 \text{ cm}^2$ and neglect the contribution of the wall to the received SNR.

C. Impact of the system parameters on the network performance

In Fig. 8, we measure the system performance as the number of UEs increases. The figure shows the cdf of the SNR obtained by the HOP algorithm for the case $M_1 = 32$, $M_2 = 4$, $A = 100 \text{ cm}^2$, $N = K$, and $K = [1, 2, 4, 8]$. Since the total transmitted power P_t is fixed and is divided among the users, we expect a 3-dB SNR loss as K doubles. In the figure this can be observed up to a certain value of K . However, for large K , the SNR degradation is much larger, e.g., it increases to 5 dB when moving from $K = 4$ to $K = 8$, and amounts to 22 dB when increasing K from 8 to 12. This behavior can be explained as follows. As K and N increase, the distance between adjacent IRSs becomes smaller and so does the

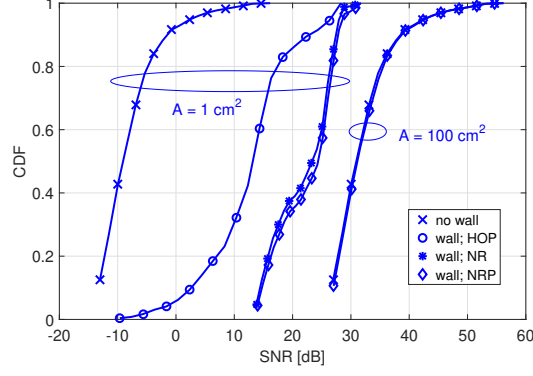


Fig. 7. Cdf of the SNR for $N = 1$, $K = 1$, $M_1 = 4$, $M_2 = 4$ and IRS area $A = [1, 100] \text{ cm}^2$. The figure shows the improvement of NRP w.r.t. HOP for small IRS area and with wall reflection.

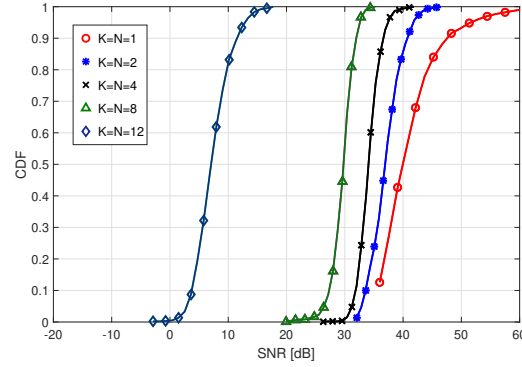


Fig. 8. Cdf of the SNR for $M_1 = 32$, $M_2 = 4$, $A = 100 \text{ cm}^2$, $N = K$, $K = [1, 2, 4, 8, 12]$, and without wall reflection. HOP algorithm.

average distance among UEs. When adjacent IRSs are very close to each other, the BS beam associated to a given user is not narrow enough to illuminate a single IRS (for an example, see the radiation pattern reported in Fig.4). Similarly, the beams reflected by the IRSs are not narrow enough to illuminate a single user. In other words, as K increases, many channels become “almost” linearly dependent, making the channel matrix ill conditioned, with many eigenvalues close to 0. Then, the pseudoinverse \mathbf{H}^+ in (24) has large eigenvalues which has the effect of reducing the SNR.

The effect of user densification is further investigated in Fig. 9, where we plot the average SNR at the UEs versus K , for different ULA sizes at the BS and at the UEs. For a given size M_1 of the BS ULA, the curves show a regular behavior for small number of UEs K , with a 3dB loss as K doubles. Instead, for larger values of K , we observe a significant performance drop, due to the reason explained above. More in detail, in the considered scenario, the bottleneck is the first hop, from the BS to the IRSs. Indeed, when the number of IRSs K

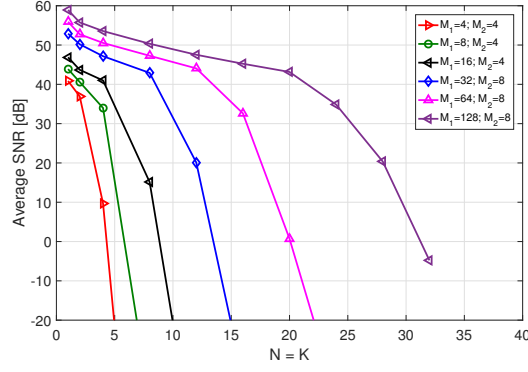


Fig. 9. Average SNR [dB] plotted versus the number of users, $K = N$, as M_1 and M_2 vary. The IRSs' area is $A = 100 \text{ cm}^2$

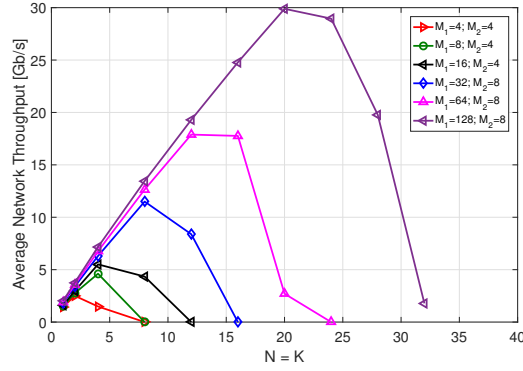


Fig. 10. Average Network Throughput R [Gbit/s] versus the number of users, $K = N$ as M_1 and M_2 vary. The IRSs' area is $A = 100 \text{ cm}^2$.

becomes too large, some of the IRSs are seen from the BS under similar angles. As an example, for $M_1 = 128$, the first-null beamwidth of the BS beam is about 1.75° . However, for $K = 24$, the angular separation between the sixteenth and the seventeenth IRS (from the left) is already lower than that, and decreases further for the rightmost IRSs. It means that there are as many as nine IRSs the BS cannot tell apart from their neighbors. Hence, the SNR loss. The second hop is less critical, since the first-null beamwidth of the IRS reflected beam, as already said, is about 2° and users are typically seen by the IRSs with a larger angular spread. We highlight that this conclusion holds for the considered geometry, while it might not hold in other scenarios.

The overall system performance can also be measured in terms of the average network throughput, defined as $T = KB\mathbb{E}[R]$, where B is the signal bandwidth and R is the spectral efficiency in (25) (equal for all users). Fig. 10 shows the average network throughput as a function of the number of supported users, for various choices of the ULAs sizes M_1 and

M_2 . For each pair (M_1, M_2) , there is an optimal value of K , K^* , which maximizes the throughput. For example, with $M_1 = 128$ and $M_2 = 8$, $K^* = 20$ and a sum rate of about 30 Gb/s can be achieved. The value of K^* lies essentially at the “knee” of the curves of Fig. 9. Also, we observe that doubling M_1 has the effect of halving the first-null beamwidth of the BS beam, thus allowing twice as many IRSs to be efficiently supported in the system, and this implies an almost doubled peak network throughput.

As a conclusion, the number of users K^* corresponding to the peak network throughput can be considered the capacity of the system. For such number of users, we serve as many users as possible without compromising the performance, because of the essentially interference-free channels established from the BS to the users. For this IRS-assisted quasi-orthogonal space-division multiple-access system, capacity is increased by increasing the size of the arrays at the BS and the UEs, and the area of the meta-surfaces.

IX. CONCLUSIONS

In this paper, we have derived a comprehensive mathematical model describing an IRS-assisted wireless network operating in the sub-THz or THz frequency bands. In such bands, for narrow signal beams, multipath-free LoS propagation can be assumed for all links. Our model is very general, as it assumes that all network nodes are equipped with multiple antennas, and takes into account the contribution of the signal reflected by large solid objects (e.g., a wall).

Capitalizing on this network model, we have expressed in simple terms the SRE optimization, supposing that the BS performs zero-forcing decoder. Such formulation consists in the maximization of the SNR received at the UE, whereas the optimization variables are the electronic rotations and the phase shifts for all IRSs, as well as the steering angles of the UE ULAs.

The approximate solution of the optimization problem has been carried out in different ways. A Newton-Raphson approach represents a method with a good accuracy, although with a comparatively high complexity. For application to realistically sized systems, a suboptimal, low-complexity heuristic algorithm is proposed, which is based on an association of users to surfaces.

Numerical results provide insight on a certain number of facts. First, if surfaces are large enough (e.g. 100 cm² in our setup), the wall reflection can be neglected. Second, with a sufficiently large number of antennas at the BS, the heuristic algorithm based on the Hungarian algorithm performs same as the Newton-Raphson approach. Third, with enough

antennas at the BS and at the UEs, user channels are orthogonal, up to a certain optimal value of K , the number of users, which is the capacity of our system. Within the capacity, users are served by the system without power waste, since the precoder tends to send all the power in the direction of the user channels, with a sort of equalization of the received SNRs.

APPENDIX A

ASYMPTOTIC EXPRESSION OF THE CHANNEL MATRIX $\tilde{\mathbf{H}}$

By using the definitions of the matrices $\mathbf{H}_n^{(2)}$, $\bar{\Theta}_n$, and $\mathbf{H}_n^{(1)}$, the vector $\mathbf{f}_k^H \tilde{\mathbf{H}}_k$ appearing in (7) can be rewritten as

$$\begin{aligned} \mathbf{f}_k^H \tilde{\mathbf{H}}_k &= \sum_{n=1}^N \frac{t_{k,n}}{L_n} \left(\mathbf{1}_{L_n}^T \otimes \mathbf{u}_{k,n}^{(2)} \right)^H (\mathbf{I}_{L_n} \otimes \bar{\Theta}_n) (\mathbf{1}_{L_n} \otimes \mathbf{u}_n^{(1)}) \mathbf{v}_n^{(1)H} + \mathbf{f}_k^H \mathbf{H}_k^{(3)} \\ &= \sum_{n=1}^N t_{k,n} \left(\mathbf{u}_{k,n}^{(2)H} \bar{\Theta}_n \mathbf{u}_n^{(1)} \right) \mathbf{v}_n^{(1)H} + t_k \mathbf{v}_k^{(3)H}, \end{aligned} \quad (40)$$

where, by recalling the expressions for $c_n^{(1)}$ and $c_{k,n}^{(2)}$ and that $A_n = L_n^2 \Delta^2 \lambda^2$ we defined

$$t_{k,n} \triangleq b_{k,n} \rho_n c_n^{(1)} c_{k,n}^{(2)} = \frac{b_{k,n} \rho_n A_n \sqrt{M_1 M_2}}{(4\pi)^2 d_n^{(1)} d_{k,n}^{(2)}} e^{-j \frac{2\pi}{\lambda} (d_n^{(1)} + d_{k,n}^{(2)})}, \quad (41)$$

$t_k \triangleq b_k \rho^{\text{wall}} c_k^{(3)}$, $b_{k,n} \triangleq \mathbf{f}_k^H \mathbf{w}_{k,n}^{(2)}$, and $b_k \triangleq \mathbf{f}_k^H \mathbf{w}_k^{(3)}$. Furthermore, by recalling the definitions of $\mathbf{u}_n^{(1)}$, $\mathbf{u}_{k,n}^{(2)}$ and $\bar{\Theta}_n$, and by assuming uniform illumination of the meta-surface we get

$$\begin{aligned} \mathbf{u}_{k,n}^{(2)H} \bar{\Theta}_n \mathbf{u}_n^{(1)} &= \frac{e^{j\psi_n}}{L_n} e^{j\pi\Delta(L_n-1)s_{k,n}} \sum_{\ell=1}^{L_n} e^{-j2\pi\Delta(\ell-1)s_{k,n}} \\ &= \frac{e^{j\psi_n}}{L_n} \frac{\sin(\pi\Delta L_n s_{k,n})}{\sin(\pi\Delta s_{k,n})} \\ &= e^{j\psi_n} \frac{\text{sinc}(\Delta L_n s_{k,n})}{\text{sinc}(\Delta s_{k,n})}, \end{aligned} \quad (42)$$

where $s_{k,n} = \sin \phi_n^{(1)} - \sin \phi_{k,n}^{(2)} - q_n$. Then,

$$\mathbf{f}_k^H \tilde{\mathbf{H}}_k = \sum_{n=1}^N t_{k,n} e^{j\psi_n} \frac{\text{sinc}(\Delta L_n s_{k,n})}{\text{sinc}(\Delta s_{k,n})} \mathbf{v}_n^{(1)H} + t_k \mathbf{v}_k^{(3)H}. \quad (43)$$

Now, as L_n increases, while the area A_n remains constant, we have $\lim_{L_n \rightarrow \infty} \text{sinc} \left(\sqrt{\frac{A_n}{L_n^2 \lambda^2}} s_{k,n} \right) = 1$. It follows that $\lim_{L_n \rightarrow \infty} \mathbf{f}_k^H \tilde{\mathbf{H}}_k = \sum_{n=1}^N t_{k,n} \text{sinc} \left(\sqrt{\frac{A_n}{\lambda^2}} s_{k,n} \right) e^{j\psi_n} \mathbf{v}_n^{(1)H} + t_k \mathbf{v}_k^{(3)H}$. Since the vector $\mathbf{f}_k^H \tilde{\mathbf{H}}_k$ is the k -th row of the matrix $\tilde{\mathbf{H}}$ we can write

$$\begin{aligned} \mathbf{H} &= \lim_{L_1, \dots, L_N \rightarrow \infty} \tilde{\mathbf{H}} = \mathbf{M} \Psi \mathbf{V}^{(1)H} + \mathbf{T} \mathbf{V}^{(3)H}, \\ [\mathbf{M}]_{k,n} &= \frac{b_{k,n} \rho_n A_n \sqrt{M_1 M_2}}{e^{j \frac{2\pi}{\lambda} (d_n^{(1)} + d_{k,n}^{(2)})} 4\pi d_n^{(1)} d_{k,n}^{(2)}} \text{sinc} \left(\sqrt{\frac{A_n}{\lambda^2}} s_{k,n} \right), \end{aligned} \quad (44)$$

$\Psi = \text{diag}(e^{j\psi_1}, \dots, e^{j\psi_N})$, $\mathbf{V}^{(1)} = [\mathbf{v}_1^{(1)}, \dots, \mathbf{v}_N^{(1)}]$, $\mathbf{V}^{(3)} = [\mathbf{v}_1^{(3)}, \dots, \mathbf{v}_K^{(3)}]$, and $\mathbf{T} = \text{diag}(t_1, \dots, t_K)$.

Finally, by recalling the expressions for \mathbf{f}_k and $\mathbf{w}_k^{(3)}$ we obtain

$$b_{k,n} \triangleq \frac{\text{sinc}(\Delta_2 M_2 (\sin \alpha_k - \sin \zeta_{k,n}))}{\text{sinc}(\Delta_2 (\sin \alpha_k - \sin \zeta_{k,n}))}; \quad b_k \triangleq \frac{\text{sinc}(\Delta_2 M_2 (\sin \alpha_k - \sin \zeta_k))}{\text{sinc}(\Delta_2 (\sin \alpha_k - \sin \zeta_k))}. \quad (45)$$

APPENDIX B

DERIVATION OF ∇f AND \mathcal{H}

We are interested in computing the gradient and the Hessian of the term $\|\mathbf{H}^+ \mathbf{Q}^{1/2}\|_{\text{F}}^2$ appearing in (24) where $\mathbf{H} = \mathbf{M}\Psi\mathbf{V}^{(1)\text{H}} + \mathbf{T}\mathbf{V}^{(3)\text{H}}$. First of all, we define $\mathbf{K} = \mathbf{H}\mathbf{H}^{\text{H}}$ and we observe that $\|\mathbf{H}^+ \mathbf{Q}^{1/2}\|_{\text{F}}^2 = \text{Tr}\{\mathbf{K}^{-1}\mathbf{Q}\}$. Let $\boldsymbol{\delta} = [\delta_1, \dots, \delta_N]^{\text{T}}$, $\boldsymbol{\psi} = [\psi_1, \dots, \psi_N]^{\text{T}}$, and $\boldsymbol{\alpha} = [\alpha_1, \dots, \alpha_K]^{\text{T}}$, be the vectors of variables to be optimized. Then we can define $f(\boldsymbol{\delta}, \boldsymbol{\psi}, \boldsymbol{\alpha}) \triangleq \text{Tr}\{\mathbf{K}^{-1}\mathbf{Q}\}$. Let x be a generic argument of the function $f(\cdot)$, and let \mathbf{A} be a matrix. Then we define $\frac{\partial \mathbf{A}}{\partial x} = \mathbf{A}_{(x)}$. Also, the first derivative of $f(\cdot)$ w.r.t. x is given by

$$\begin{aligned} \frac{\partial f}{\partial x} &= \sum_{i,j} \frac{\partial \text{Tr}\{\mathbf{K}^{-1}\mathbf{Q}\}}{\partial K_{i,j}} \frac{\partial K_{i,j}}{\partial x} \\ &= \sum_{i,j} \text{Tr} \left\{ \frac{\partial \text{Tr}\{\mathbf{Y}^{-1}\mathbf{Q}\}}{\partial \mathbf{Y}} \bigg|_{\mathbf{Y}=\mathbf{K}} \frac{\partial \mathbf{K}}{\partial K_{i,j}} \right\} \frac{\partial K_{i,j}}{\partial x} \\ &= - \sum_{i,j} \text{Tr} \left\{ (\mathbf{K}^{-1}\mathbf{Q}\mathbf{K}^{-1})^{\text{T}} \mathbf{J}^{(i,j)} \right\} \frac{\partial K_{i,j}}{\partial x}, \end{aligned} \quad (46)$$

where the last equality comes from [34, Eq. (121)]. In (46), \mathbf{Y} is a matrix whose entries are independent variables, and $\mathbf{J}^{(i,j)} = \frac{\partial \mathbf{K}}{\partial K_{i,j}}$ represents the structure of the matrix \mathbf{K} . The matrix \mathbf{K} is complex Hermitian, thus $[\mathbf{J}^{(i,j)}]_{m,n} = 0$ for $(m,n) \neq (i,j)$ and $(m,n) \neq (j,i)$. Clearly $[\mathbf{J}^{(i,j)}]_{i,j} = 1$, whereas² $[\mathbf{J}^{(i,j)}]_{j,i} = \frac{\partial K_{j,i}}{\partial K_{i,j}} = \frac{\partial K_{i,j}^*}{\partial K_{i,j}} = 0$. Then, from (46) we obtain

$$\begin{aligned} \frac{\partial f}{\partial x} &= - \sum_{i,j} [\mathbf{K}^{-1}\mathbf{Q}\mathbf{K}^{-1}]_{j,i} \frac{\partial K_{i,j}}{\partial x} \\ &= - \text{Tr} \left\{ \mathbf{K}^{-1}\mathbf{Q}\mathbf{K}^{-1} \frac{\partial \mathbf{K}}{\partial x} \right\} \\ &= - \text{Tr} \left\{ \mathbf{Z}\mathbf{K}_{(x)} \right\}, \end{aligned} \quad (47)$$

where $\mathbf{Z} \triangleq \mathbf{K}^{-1}\mathbf{Q}\mathbf{K}^{-1}$. Now let y be another argument of the function $f(\boldsymbol{\delta}, \boldsymbol{\psi}, \boldsymbol{\varphi})$. The second mixed derivative of $f(\cdot)$ is given by

$$\frac{\partial^2 f}{\partial x \partial y} = - \frac{\partial}{\partial y} \text{Tr} \left\{ \mathbf{Z}\mathbf{K}_{(x)} \right\} = - \text{Tr} \left\{ \frac{\partial \mathbf{Z}}{\partial y} \mathbf{K}_{(x)} + \mathbf{Z} \frac{\partial}{\partial y} \mathbf{K}_{(x)} \right\}. \quad (48)$$

²Here, in order to handle complex differentiation of non analytic functions we use the definition of Wirtinger derivatives [35].

Now observe that $\frac{\partial \mathbf{Z}}{\partial y} = -2\mathbf{Z}\mathbf{K}_{(y)}\mathbf{K}^{-1}$. Thus we obtain

$$\frac{\partial^2 f}{\partial x \partial y} = -\text{Tr} \{ -2\mathbf{Z}\mathbf{K}_{(y)}\mathbf{K}^{-1}\mathbf{K}_{(x)} + \mathbf{Z}\mathbf{K}_{(xy)} \} = \text{Tr} \{ \mathbf{Z}(2\mathbf{K}_{(y)}\mathbf{K}^{-1}\mathbf{K}_{(x)} - \mathbf{K}_{(xy)}) \} \quad (49)$$

where $\mathbf{K}_{(xy)} = \frac{\partial}{\partial y}\mathbf{K}_{(x)}$. The Hessian of $f(\cdot)$ is then defined in terms of the derivatives of \mathbf{K}

$$\mathbf{K}_{(x)} = \frac{\partial}{\partial x}\mathbf{H}\mathbf{H}^H = \mathbf{H}_{(x)}\mathbf{H}^H + \mathbf{H}\mathbf{H}_{(x)}^H = 2\Re \{ \mathbf{H}_{(x)}\mathbf{H}^H \} , \quad (50)$$

and, thus $\mathbf{K}_{(xy)} = 2\Re \{ \mathbf{H}_{(xy)}\mathbf{H}^H + \mathbf{H}_{(x)}\mathbf{H}_{(y)}^H \}$. The derivatives of \mathbf{H} are easy to obtain from (15). In particular the matrix \mathbf{M} depends on both δ and on α , the matrix Ψ depends on ψ only, and \mathbf{T} depends on α only. The obtained expressions are quite cumbersome and, for simplicity, are not reported here.

REFERENCES

- [1] J. Qiao and M.-S. Alouini, "Secure transmission for intelligent reflecting surface-assisted mmwave and terahertz systems," *IEEE Wireless Communications Letters*, vol. 9, pp. 16–32, 2020.
- [2] I. F. Akyildiz, J. M. Jornet, and C. Han, "Terahertz band: next frontier for wireless communications," *Physical Communication*, vol. 12, pp. 16–32, 2014.
- [3] C. Pan, H. Ren, K. Wang, W. Xu, M. ElKashlan, A. Nallanathan, and L. Hanzo, "Multicell MIMO communications relying on intelligent reflecting surfaces," *IEEE Transactions on Wireless Communications*, vol. 19, 2020.
- [4] M. Di Renzo *et al.*, "Smart radio environments empowered by reconfigurable AI meta-surfaces: an idea whose time has come," *EURASIP Journal*, 2019.
- [5] Q. Wu and R. Zhang, "Towards smart and reconfigurable environment: Intelligent reflecting surface aided wireless network," *IEEE Communications Magazine*, pp. 106–112, January 2020.
- [6] C. Liaskos, S. Nie, A. Tsioliaridou, A. Pitsillides, S. Ioannidis, and I. Akyildiz, "A new wireless communication paradigm through software-controlled metasurfaces," *IEEE Communications Magazine*, 2018.
- [7] X. Tan, Z. Sun, J. M. Jornet, and D. Pados, "Increasing indoor spectrum sharing capacity using smart reflect-array," in *IEEE ICC*, 2016.
- [8] C. Liaskos, A. Tsioliaridou, A. Pitsillides, S. Ioannidis, and I. Akyildiz, "Using any surface to realize a new paradigm for wireless communications," *Communications of the ACM*, 2018.
- [9] M. Alsharif, A. K. amd M.A. Albreem, S. Chaudhry, M. Zia, and S. Kim, "Sixth generation (6G) wireless networks: Vision, research activities, challenges and potential solutions," *Symmetry*, vol. 12, no. 4:676, 2020.
- [10] M. A. Saeidi, M. J. Emadi, H. Masoumi, M. R. Mili, D. W. K. Ng, and I. Krikidis, "Weighted sum-rate maximization for multi-IRS-assisted full-duplex systems with hardware impairments," *arXiv:2010.01339*, vol. 9, no. 10, 2020.
- [11] C. Pan, H. Ren, K. Wang, W. Xu, M. ElKashlan, A. Nallanathan, and L. Hanzo, "Multicell MIMO communications relying on intelligent reflecting surfaces," *arXiv:1907.10864v4*, 2020.
- [12] Z. Li, M. Hua, Q. Wang, and Q. Song, "Weighted sum-rate maximization for multi-IRS aided cooperative transmission," *IEEE Wireless Communications Letters*, vol. 9, no. 10, pp. 1620–1624, 2020.
- [13] A. A. M. Saleh and R. Valenzuela, "A statistical model for indoor multipath propagation," *IEEE Journ. Selected Areas in Commun.*, vol. 5, no. 2, pp. 128–137, Feb. 1987.
- [14] V. Raghavan, J. Cezanne, S. Subramanian, A. Sampath, and O. Koymen, "Beamforming tradeoffs for initial ue discovery in millimeter-wave MIMO systems," *IEEE Journal of Selected Topics in Signal Processing*, vol. 10, no. 3, pp. 543–559, April 2016.

- [15] Y. Xing, O. Kanhere, S. Ju, and T. S. Rappaport, "Indoor wireless channel properties at millimeter wave and sub-terahertz frequencies," *IEEE Global Communications Conference*, 2019.
- [16] N. Yu, P. Genevet, M. A. Kats, F. Aieta, J.-P. Tetienne, F. Capasso, and Z. Gaburro, "Light propagation with phase discontinuities: generalized laws of reflection and refraction," *Science*, 2011.
- [17] A. ElMossallamy, H. Zhang, L. Song, K. G. Seddik, Z. Han, and G. Y. Li, "Reconfigurable intelligent surfaces for wireless communications: Principles, challenges, and opportunities," *arXiv:2005.00938v1*, 2020.
- [18] S. Gong, X. Lu, D. T. Hoang, D. Niyato, L. Shu, D. I. Kim, and Y.-C. Liang, "Toward smart wireless communications via intelligent reflecting surfaces: A contemporary survey," *IEEE Communications Surveys & Tutorials*, vol. 22, no. 4, 2020.
- [19] Q. Wu, S. Zhang, B. Zheng, C. You, and R. Zhang, "Intelligent reflecting surface aided wireless communications: A tutorial," *IEEE Transactions on Communications*, 2021.
- [20] J. He, H. Wymeersch, L. Kong, O. Silvén, and M. Juntti, "Large intelligent surface for positioning in millimeter wave mimo systems," in *2020 IEEE 91st Vehicular Technology Conference (VTC2020-Spring)*, 2020, pp. 1–5.
- [21] P. Wang, J. Fang, X. Yuan, Z. Chen, and H. Li, "Intelligent reflecting surface-assisted millimeter wave communications: Joint active and passive precoding design," *IEEE Transactions on Vehicular Technology*, vol. 69, no. 12, pp. 14 960–14 973, 2020.
- [22] O. Özdoğan, E. Björnson, and E. G. Larsson, "Intelligent reflecting surfaces: Physics, propagation, and pathloss modeling," *IEEE Wireless Commun. Lett.*, vol. 9, no. 5, pp. 581–585, 2020.
- [23] Q. Wu and R. Zhang, "Intelligent reflecting surface enhanced wireless network: Joint active and passive beamforming design," *IEEE Globecom*, pp. 1–6, 2018.
- [24] M.-M. Zhao, Q. Wu, M.-J. Zhao, and R. Zhang, "Intelligent reflecting surface enhanced wireless network: Two-timescale beamforming optimization," *IEEE Trans. Wireless Commun.*, 2021.
- [25] X. Li, J. Fang, F. Gao, and H. Li, "Joint active and passive beamforming for intelligent reflecting surface-assisted massive MIMO systems," *arXiv: 1912.00728v1*, 2019.
- [26] M. Dunna, C. Zhang, D. Sievenpiper, and D. Bharadia, "ScatterMIMO: Enabling virtual MIMO with smart surfaces," *MobiCom '20: Proceedings of the 26th Annual International Conference on Mobile Computing and Networking*, 2020.
- [27] Y. Han, S. Zhang, L. Duan, and R. Zhang, "Cooperative double-IRS aided communication: Beamforming design and power scaling," *IEEE Wireless Communications Letters*, vol. 9, no. 8, pp. 1206–1210, 2020.
- [28] M. D. Renzo, F. H. Danufane, X. Xi, J. de Rosny, and S. Tretyakov, "Analytical modeling of the path-loss for reconfigurable intelligent surfaces – anomalous mirror or scatterer?" *arXiv:2001.10862v1*, 2020.
- [29] J. Xu, W. Xu, and A. L. Swindlehurst, "Discrete phase shift design for practical large intelligent surface communication," *Proc. IEEE Pac. Rim Conf. Commun. Comput. Signal Process. (PACRIM)*, p. 1–5, Aug. 2019.
- [30] A. Tarable, F. Malandrino, L. Dossi, R. Nebuloni, G. Virone, and A. Nordio, "Meta-surface optimization in 6G sub-THz communications," in *IEEE ICC*, 2020.
- [31] C. Huang, A. Zappone, G. C. Alexandropoulos, M. Debbah, and C. Yuen, "Reconfigurable intelligent surfaces for energy efficiency in wireless communication," *IEEE Transactions on Wireless Communications*, 2019.
- [32] H. W. Kuhn, "The hungarian method for the assignment problem," *Naval Research Logistics Quarterly*, vol. 2, no. 1–2, pp. 83–97, 1955. [Online]. Available: <https://onlinelibrary.wiley.com/doi/abs/10.1002/nav.3800020109>
- [33] ITU-T, "Effects of building materials and structures on radiowave propagation above about 100 MHz," International Telecommunication Union, Recommendation P.2060-1, 2015.
- [34] K. B. Petersen, M. S. Pedersen, J. Larsen, K. Strimmer, L. Christiansen, K. Hansen, L. He, L. Thibaut, M. Baro, S. Hattinger *et al.*, "The matrix cookbook," *Kgs. Lyngby, Denmark: Tech. Univ. Denmark*, 2006.
- [35] R. Remmert, *Theory of Complex Functions*. Springer-Verlag, 1998.